



## EG-ICE 2025 GLASGOW

# Enhancing Bridge Defect Semantic Segmentation Via Synthetic Point Cloud Data Generation

YUANSHENG XU<sup>1</sup>, ANDRE JESUS<sup>1</sup>, CRAIG HANCOCK<sup>1</sup>, MINGZHU WANG<sup>2</sup>

<sup>1</sup>School of Architecture, Building and Civil Engineering, Loughborough University, Loughborough, United Kingdom

<sup>2</sup>School of Architecture and Civil Engineering, City University of Hong Kong, Hong Kong, China

### ABSTRACT:

The structural integrity of bridges is critical for modern transportation systems, yet current methods for defect detection and segmentation on curved concrete surfaces remain limited in precision and cost-effectiveness. Data scarcity is also a significant problem. This study addresses these challenges by proposing a framework leveraging synthetic data generation and a Surface Normal Enhanced PointConv (SNEPointConv) model for bridge defect semantic segmentation. The proposed approach includes a low-cost method for generating synthetic cracks and spalling defects that mimic real-world bridge defect geometries, enabling effective training of deep learning models. Additionally, the SNEPointConv model integrates normal vector enhancements to improve feature extraction from irregular point clouds. Experiments demonstrate the feasibility of using synthetic datasets for defect semantic segmentation, bridging the gap between real-world defect characteristics and digital twin applications for structural health monitoring. Key contributions include the development of scalable synthetic defect data generation techniques, improved defect segmentation accuracy through feature enhancement, and a comprehensive exploration of the effectiveness of synthetic dataset in model training.

### KEYWORDS:

Defect Detection, Point Cloud, Semantic Segmentation, Synthetic Data Generation, Point Convolution

## 1. INTRODUCTION

Bridges are critical to modern transportation systems and are susceptible to degradation due to improper maintenance, overloading, chemical corrosion, and sudden load bursts (Han et al., 2023). The manifestation of defects is frequently perceived as a harbinger of structural degradation and even an antecedent to catastrophic failure. Among the 12 recognized types of bridge defects, cracks and spalling are the most prevalent and consequential (Flotzinger et al., 2024). Particularly, the bridge pier serves as a pivotal structural component,

transferring vertical and horizontal forces from decks to the foundation, ensuring overall structural stability (Burmister, 1938). Despite its critical role, current research in bridge structural health monitoring (SHM) predominantly emphasizes defect semantic segmentation on flat surfaces, with limited attention given to the stability and defect characterization of bridge piers (Valença et al., 2017; Bolourian et al., 2022).

Traditional defect detection, relying on manual inspections, is labor-intensive, time-consuming, and fraught with inaccuracies (Lv & Brilakis, 2019). While on-site inspections necessitating road

closures mitigate some risks, they induce significant economic losses and fail to eliminate occupational hazards (Metni & Hamel, 2007; The Vertical Press, 2015). In essence, manual methods are error-prone, require specialized expertise, and expose inspectors to elevated risks (Nishikawa et al., 2012).

Advancements in sensing technologies and artificial intelligence (AI) have driven significant progress in defect classification, detection, and semantic segmentation (Cheng & Wang, 2018; Wang & Cheng, 2019; Rodrigo et al., 2022), namely via the structural health monitoring (SHM) discipline, which can provide stakeholders with early warning and thus avert catastrophic collapse. While state-of-the-art 2D methods based on visual data achieve over 95% accuracy in defect recognition and segmentation (Chen et al., 2022), their lack of depth information limits their applicability in 3D contexts such as Building Information Modeling (BIM).

Meanwhile, it is imperative to construct an integrated model capable of synergizing data from heterogeneous sensors to establish a comprehensive framework for full-cycle SHM. The inherent limitations of current imaging modalities render them insufficient for the precise reconstruction of three-dimensional models, thereby constraining their utility in advanced applications. Furthermore, the advent of robot-assisted bridge maintenance necessitates meticulous navigation, including precise localization and adept obstacle avoidance. However, the reliance on two-dimensional planar information presents an intrinsic impediment to achieving nuanced perception in complex three-dimensional environments.

To bridge this gap, semi-automated inspection approaches leveraging 3D Light Detection and Ranging (LiDAR) and advanced imaging have emerged, facilitated by innovations in point cloud acquisition and deep learning (Wang et al., 2024). These methods enable defect detection, classification, and segmentation, often integrating color and geometric features with clustering algorithms to enhance textural damage detection (Mohammadi et al., 2019; Hou et al., 2017). A significant impediment to the advancement of point cloud-based defect semantic segmentation is the scarcity of existing 3D datasets (Shao et al., 2024).

Synthetic data generation offers a viable alternative for model training and validation. Mehrdad et al. (2019) introduced a voxel-based method for simulating concrete cracks and spalling using 3D CAD modeling. While effective, this approach struggles to accurately represent fine cracks within the 3D spatial domain. Building upon these efforts, Shao et al. (2024) integrated numerical simulation and 3D surface reconstruction

using RGB images captured from synthetic cameras positioned at various angles, rendered through the Blender engine. Despite its innovative framework, this method is constrained by the data acquisition process that needs to be tailored to the reconstruction algorithm, limiting the model's generalizability to complex scenarios. Additionally, approaches relying on multi-view reconstruction often require redundant input data, and the need to transform data across formats introduces errors that further compromise the fidelity of the generated datasets.

Despite progress, limitations in laser scanner accuracy and state-of-the-art (SOTA) models have confined crack width detection to 1-4 mm (Valença et al., 2017), whereas cracks with width as small as 0.3-1 mm are classified as structural defects indicative of deflection, creep, or overloading (Thomas et al., 2008). Current methods fall short of meeting stringent inspection standards (being able to detect 0.2mm-wide crack).

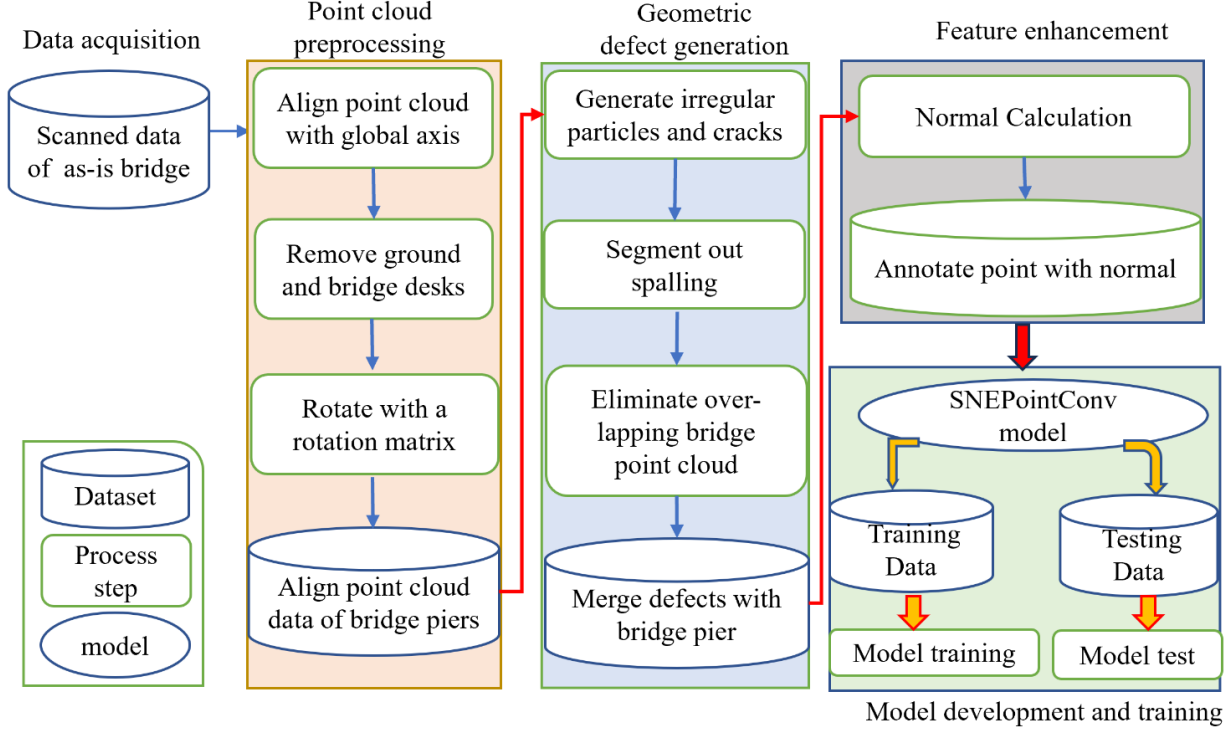
Therefore, this study aims to enhance semantic segmentation of bridge defects by addressing the data scarcity problem. A framework is proposed to generate synthetic data of bridge defects, which will be integrated with real-world bridge pier point clouds to train the defect semantic segmentation model. Meanwhile, feature enhancement is performed and a Surface Normal Enhanced PointConv (SNEPointConv) model based on Point Convolution (Wu et al., 2018) is proposed to improve the robustness of bridge defect segmentation.

## 2. THE PROPOSED METHODOLOGY FRAMEWORK

This paper proposes a framework for generating synthetic point cloud data for bridge defect semantic segmentation. As shown in Figure 1, the framework consists of four components: data acquisition and preprocessing, geometric defect generation, feature enhancement, and model development and training. Details of each component will be introduced in the following.

### 2.1 POINT CLOUD ACQUISITION AND PREPROCESSING

A primitive bridge point cloud is obtained by scanning an as-is bridge. To streamline subsequent procedures, the point clouds must be rotated to align with the XOY plane. This is achieved by left-multiplying the point cloud coordinate ( $P = \{p_i = (x_i, y_i, z_i)\} \in R^3$ ) with a rotation matrix. To simplify the rotation process, a rotation matrix could be composed as a sequence of three basic rotations around the x-, y-, and z-axes of the right-hand Cartesian coordinate system.



**2.2 GEOMETRIC DEFECT GENERATION**

First, assume a two-dimensional point cloud crack lies on the  $XOY$  plane with a  $z$ -coordinate of 0. Its basic shape is derived by modifying 2D Perlin noise. While the generated  $(x, y)$  vertices exhibit randomness and heterogeneity, they lack precise geometric correlation between crack width and length, limiting their resemblance to real concrete cracks. To integrate the calculation,  $y$  coordinate value is calculated through Equation (1).

$$y = y_{noise} + L \cdot \left(1 - \frac{\sqrt{r_x^2 - x^2}}{r_x}\right) \quad (1)$$

where  $r_x$  is the ellipse minor axis radius,  $x$  is the  $x$ -coordinate value of crack point,  $L$  is the length of crack,  $y_{noise}$  is the Perline noise value.

Figure 1. The proposed methodology framework

Crack width typically varies along its length. Here, the width is sampled from a normal distribution (mean 1.5, standard deviation 0.5) relative to the decreasing  $x$ -coordinate. The  $z$ -coordinate is determined by a local surface fitting method (Piegl & Tiller, 1997), and a typical generated crack is illustrated in Figure 2.



Figure 2. A synthetic crack geometric shape

Second, spalling generation process is built based on a method of particle shape generation with spherical harmonics (Wei et al., 2018). The macroscopic size of the particles is mainly affected by length ( $d_1$ ), width ( $d_2$ ) and height ( $d_3$ ), and their

roundness and roughness are controlled by normalized spherical descriptors  $d_{2-8}/d_1$  and  $d_{9-15}/d_1$ . Overall, as the aspect ratio decreases, the particles become more elongated. When  $d_{2-8}/d_1$  and  $d_{9-15}/d_1$  increase, the irregularity of the particle surface increases accordingly.

The irregular particles generated will be transformed from mesh to point clouds, which will be arbitrarily placed on a primitively collected bridge pier point clouds in 3D space. As depicted in Figure 3, an irregular sphere (represented by red and yellow points) and a segment of the collected bridge pier point cloud are positioned in 3D space with partial overlap. As defects typically appear on the concave side of a bridge pier. the irregular sphere above the concave fitting surface needs to be eliminated.

Third, a pier surface function  $F(x, y, z) = 0$  is calculated by a local surface fitting method (Piegl & Tiller, 1997). The portion to be eliminated for a point

cloud  $P$  of a sphere can be calculated using Equation (2).

$$p_e : z_s - F(x_s, y_s) > threshold \quad (2)$$

where  $p_e$  is the eliminated point cloud,  $x_s, y_s, z_s$  is the coordinates of a given sphere.

Based on experimental results, a threshold of -0.01 was established to guarantee the removal of all points above the fitting surface. The overlapping part between two point clouds of an irregular particle and a bridge pier will be eliminated based on occupancy calculation. For a given point, the signed distance and occupancy are only valid after the inside and outside are clearly defined. The signed distance is negative if the query point is inside the mesh. The occupancy is either -1 for points outside the mesh and 1 for points inside the mesh. And the points with an occupancy of -1 label will be eliminated.

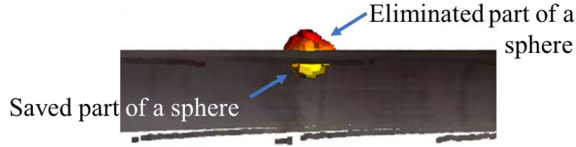


Figure 3. Relative position of a sphere and a pier point cloud

Last, the coordinate and colour information of synthetic defects and primitive bridge pier point clouds will be integrated. Initially, the synthetic defect point clouds only equip coordinates and lack colour information. Based on two key characteristics of as-is bridge defects: their colour and depth are usually darker and deeper compared to the adjacent areas (Bolourian et al., 2022). Hereby, the RGB values of defects are assigned with the biggest RGB values of bridge piers. To contract against bridge pier points, RGB value deviations between bridge pier points and defect points should be enlarged by 20%. Figure 4 lists two comparisons between synthetic defects and real-world bridge defect point clouds. The shown real bridge point cloud data is based on a case-study example, which will be detailed in the experiment Section.

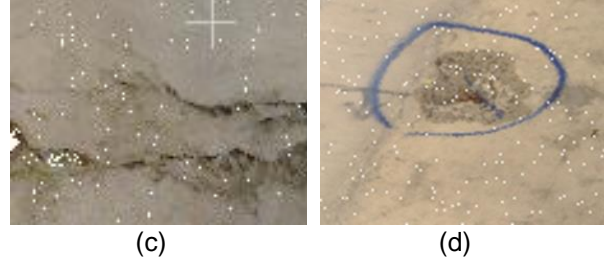
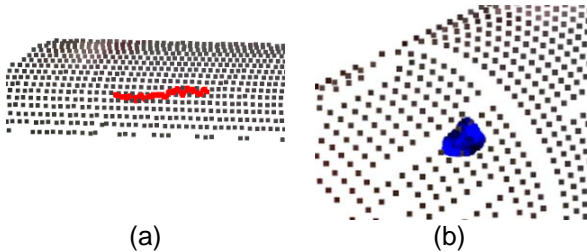


Figure 4. Synthetic and real-world bridge defect data (a) and (b) are generated crack and spalling (blue points), while (c) and (d) are real-world bridge defect point cloud data from (Bolourian et al., 2022).

### 2.3 FEATURE ENHANCEMENT

To improve the model's capability of learning defect features, a practical approach is to include normal vectors as part of input features for training the model. Let the surface function be expressed as  $F(x, y, z) = 0$ , calculated by the local surface fitting method. The normal vector for a point  $p_a$  can be computed using Equation (3) (Silverman, 2002).

$$\vec{N} = \frac{\nabla F}{\|\nabla F\|} \quad (3)$$

where  $\nabla F$  is the gradient of  $F$ ,  $\|\nabla F\|$  is the vector magnitude.

As illustrated in Figure 5, the normal vectors at the deepest point ( $\vec{N}_2$ ) and at a non-defective point ( $\vec{N}_1$ ) are orthogonal to the  $XY$  plane. Conversely, the normal vector corresponding to a defect ( $\vec{N}_i$ ) deviates from this orthogonality, being neither parallel nor perpendicular to the  $XY$  plane. Consequently, the presence of potential defects can be inferred by analyzing the variation in orientation between adjacent normal vectors.

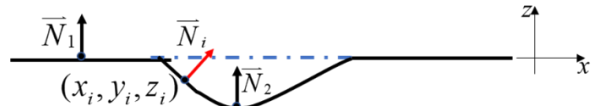
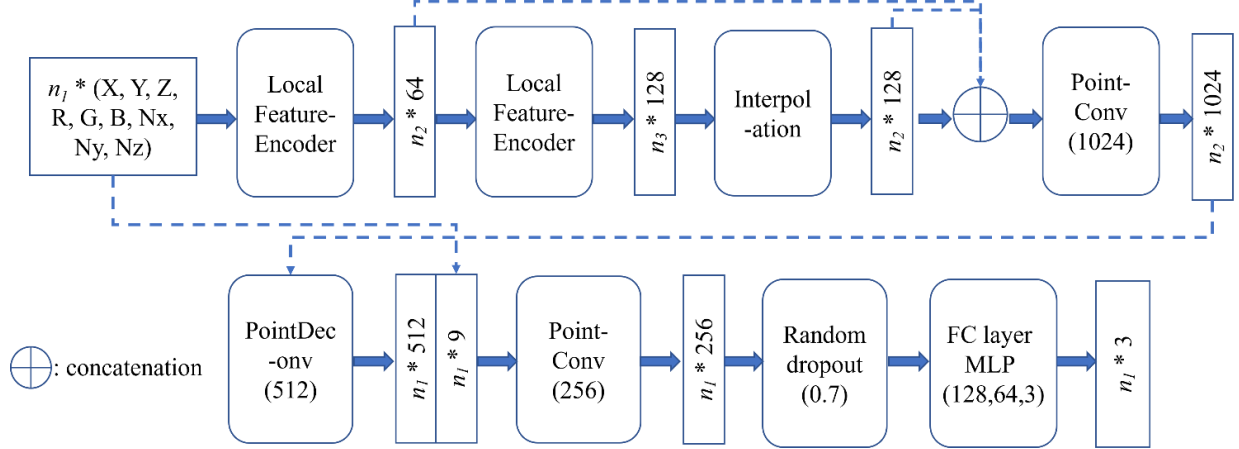


Figure 5. Vectors of a defect point and non-defect points

### 2.4 MODEL DEVELOPING AND TRAINING

The proposed network architecture, illustrated in Figure 6, consists of three principal components: PointConv modules, an interpolation module, and a multilayer perceptron (MLP) prediction module. Initially, the PointConv module facilitates the aggregation of local geometric and spatial information from the point cloud domain. Subsequently, the interpolation module propagates coarse-grained features derived from the preceding



layer to ensure continuity across the feature space. To preserve feature integrity and enhance information flow, skip connections are established between the interpolated convolutional layer and its corresponding convolutional layer of identical

dimensionality. Finally, the PointConv module is re-engaged to refine and extract the fused feature representations, culminating in the output prediction values.

Figure 6. Architecture of the SNEPointConv. This figure shows how the features are encoded and decoded via backbone.  $n$  is the number of points in each layer

Point clouds collected by current sensors exhibit significant density variation. To address this inhomogeneity, a density function is applied to weight the learned features. In a local neighbourhood  $G$ , the relative coordinates of points are denoted as  $(x_\mu, y_\mu, z_\mu)$ . The feature  $F(x + x_\mu, y + y_\mu, z + z_\mu)$  describes the local region centered at  $p=(x, y, z)$ . The weight function  $W(x_\mu, y_\mu, z_\mu)$ , approximated using a multi-layer perceptron (MLP), assigns weights to features based on relative point positions within  $G$ . A density coefficient function  $D(x_\mu, y_\mu, z_\mu)$  maps point density to corresponding coefficients, further refining feature representation. Hence the output is calculated via Equation (4).

$$F_{out} = \sum_{(x_\mu, y_\mu, z_\mu)} D(x_\mu, y_\mu, z_\mu) \bullet W(x_\mu, y_\mu, z_\mu) F_{in}(x + x_\mu, y + y_\mu, z + z_\mu)$$

### 3. EXPERIMENT RESULTS AND DISCUSSION

By applying the proposed data generation methods, this study generated 500 point clouds, representing bridge piers with embedded defects (cracks and spalling). Table 1 delineates the distribution of the generated synthetic defects alongside the corresponding number of points, while Table 2 specifies the irregular particle parameters utilized for synthetic spalling generation. The cracks exhibit lengths varying from 10 cm to 50 cm and widths ranging from 0.2 mm to 0.6 mm, respectively. The generated dataset were partitioned into subsets for model training, validation, and testing in semantic segmentation tasks.

Table 1. Dataset information

Dataset	Number of data	Defects				Non-defect Number of points
		Cracks		Spalling		
		Number of cracks	Number of points	Number of spalling	Number of points	
Training	300	1,718	128,484	1118	723,346	9,079,123
Evaluation	100	610	49,770	410	250,100	2,989,438
Testing	100	598	45,256	437	261,326	2,974,684
Total	500	4,267	223,510	1,965	1,234,772	16,133,245

Table 2. Irregular particle factors

Particles	$E_l$	$F_l$	$d_{2-g}/d_1$	$d_{9-1g}/d_1$
Spheres	[0.5,0.8]	1	[0.2,0.9]	[0.2,0.9]
Ellipsoid	[0.01,0.05]	2	[0.0,0.2]	[0.0,0.9]

For training the model, the experimental framework was established in a Pytorch-GPU 2.1.1 environment, complemented by Cuda 11.8.0 and Python 3.8. Parallelized computations were expedited via two NVIDIA 3090 GPUs. The learning rate was initially configured at  $1e-3$  and subsequently attenuated to a nadir of  $1e-5$ . Training epochs were capped at 50. To mitigate the disproportionate influence of dominant samples and features on predictive outcomes, a weighted cross-entropy loss function was employed, thereby enhancing the model's generalization capabilities.

Table 3. training and test results

Categories	Training		Evaluation		Testing	
	Accuracy (%)	IoU (%)	Accuracy (%)	IoU (%)	Accuracy (%)	IoU (%)
Crack	95.84	76.4	93.27	73.5	82.02	69.4
Spalling	96.62	87.2	94.79	82.3	82.45	74.6
Non defect	97.03	94.4	98.40	93.9	97.40	95.3

The superior performance in spalling segmentation can be attributed to its distinct geometric and visual features. Spalling is typically characterized by larger, irregular patterns with clear boundaries, making it easier for the model to distinguish. Conversely, cracks often exhibit fine, linear structures that are more challenging to detect, especially in noisy or low-resolution data. Cracks are also more prone to overlap with non-defective

The empirically derived class weights for crack, spalling, and no defect were calculated as 0.837, 0.151, and 0.011, respectively.

The experiment results (see Table 3) show that spalling segmentation consistently outperforms crack segmentation across all metrics and phases (training, evaluation, and testing). While training accuracy for both classes is relatively high, the testing accuracy and Intersection over Union (IoU) for cracks drop significantly (82.02% and 69.4%, respectively), indicating challenges in generalization. In contrast, spalling segmentation achieves much better testing performance, with an accuracy of 87.40% and IoU of 95.3%. This suggests that the model is better at identifying and segmenting spalling features compared to cracks.

regions, leading to confusion during segmentation. Additionally, the model's architecture may inherently favor larger-scale features like spalling over the finer details of cracks, as the weighting mechanisms in SNEPointConv are likely more suitable for detecting prominent geometric variations. A comparison of the generated point cloud with defects, ground truth and segmentation results were shown in Figure 7.

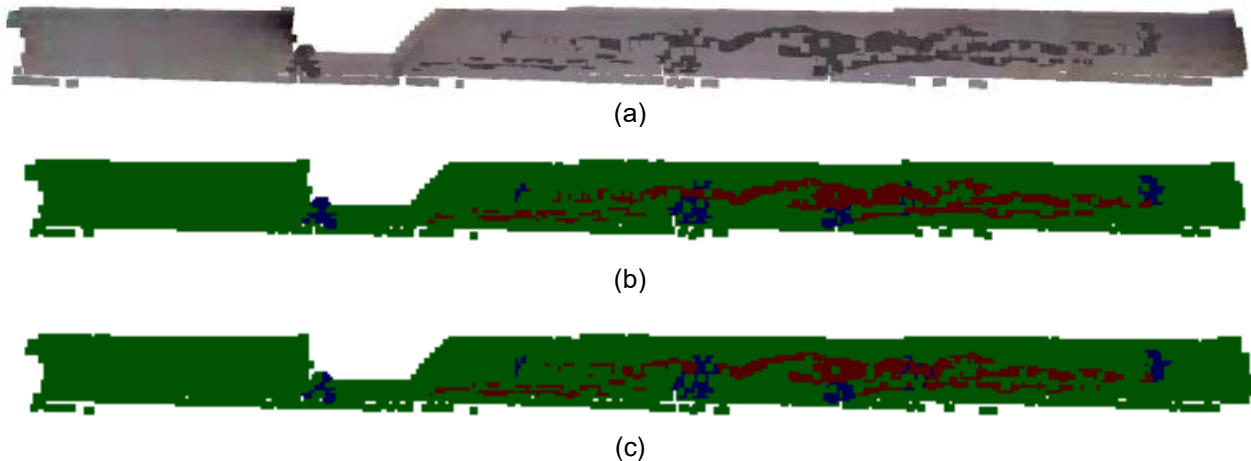


Figure 7. (a) primitive point cloud, (b) ground truth (red: crack, green: spalling and blue: bridge pier), (c) segmentation result

#### 4. CONCLUSIONS

This study presents a cost-effective and efficient

method for generating synthetic bridge defect point cloud data and integrates Surface Normal Enhanced PointConv (SNEPointConv) for enhancing defect segmentation on curved concrete surfaces. The proposed framework successfully segments cracks as narrow as 0.2 mm, addressing critical challenges in bridge structural health monitoring. While spalling segmentation outperforms crack segmentation due to its distinct geometric features, the framework demonstrates the potential for industrial applications by bridging the gap between synthetic and real-world defect datasets. The key contributions of this study include: (1) proposing a cost-effective 3D point cloud crack generation method that mimics real concrete crack geometry, (2) proposing a spherical harmonics-based spalling generation method to create irregular defects on diverse surfaces, and (3) developing a feature-enhanced PointConv model for bridge defect segmentation, demonstrating the effectiveness of the generated synthetic data to improve defect segmentation.

To further enhance the performance of bridge defect segmentation, future works could focus on (1) increasing the diversity and volume of defect data by incorporating high-resolution and real-world datasets to improve generalization, and (2) evaluating the proposed method on real-world datasets and field applications to ensure robustness and practical viability.

By addressing these areas, the proposed framework can further bridge the gap between research and industry, enhancing its applicability to structural health monitoring and other critical infrastructure assessments.

## REFERENCES

Bolourian, N., Nasrollahi, M., Bahreini, F. and Hammad, A., 2022. Point cloud-based concrete surface defect semantic segmentation. *Journal of Computing in Civil Engineering*, [online] Available at: <https://doi.org/10.1061/JCCEE5.CPENG-5009> [Accessed 10 May 2025].

Burmister, D.M., 1938. Stability of bridge piers. *Proceedings of the Eighteenth Annual Meeting of the Highway Research Board*, [online] Available at: <https://onlinepubs.trb.org/Onlinepubs/hrbproceedings/18/18Part2-008.pdf> [Accessed 10 May 2025].

Cheng, J.C.P. and Wang, M., 2018. Automated detection of sewer pipe defects in closed-circuit television images using deep learning techniques. *Automation in Construction*, 95, pp.155–171. <https://doi.org/10.1016/j.autcon.2018.08.006>.

Choi, M., Kim, S. and Kim, S., 2024. Semi-automated visualization method for visual inspection of buildings on BIM using 3D point cloud. *Journal of Building Engineering*, 81, 108017.

<https://doi.org/10.1016/j.jobe.2023.108017>.

Flotzinger, J., Rösch, P.J. and Braml, T., 2024. dacl10k: Benchmark for semantic bridge damage segmentation. In: *Proceedings of the IEEE/CVF Winter Conference on Applications of Computer Vision (WACV)*. pp.8626–8635.

Han, D., Hosamo, H., Ying, C. and Nie, R., 2023. A comprehensive review and analysis of nanosensors for structural health monitoring in bridge maintenance: Innovations, challenges, and future perspectives. *Applied Sciences*, 13(20), p.11149. <https://doi.org/10.3390/app132011149>.

Hou, T.-C., Liu, J.-W. and Liu, Y.-W., 2017. Algorithmic clustering of LiDAR point cloud data for textural damage identifications of structural elements. *Measurement*, 108, pp.77–90. <https://doi.org/10.1016/j.measurement.2017.05.032>.

Lu, R. and Brilakis, I., 2019. Digital twinning of existing reinforced concrete bridges from labelled point clusters. *Automation in Construction*, 105, 102837.

<https://doi.org/10.1016/j.autcon.2019.102837>.

Metni, N. and Hamel, T., 2007. A UAV for bridge inspection: Visual servoing control law with orientation limits. *Automation in Construction*, 17(1), pp.3–10.

Mohammadi, M.E., Wood, R.L. and Wittich, C.E., 2019. Non-temporal point cloud analysis for surface damage in civil structures. *ISPRS International Journal of Geo-Information*, 8(12), p.527. <https://doi.org/10.3390/ijgi8120527>.

Dizaji, M.S. and Harris, D.K., 2019. 3D InspectionNet: A deep 3D convolutional neural networks-based approach for 3D defect detection on concrete columns. In: *Proc. SPIE 10971, Nondestructive Characterization and Monitoring of Advanced Materials, Aerospace, Civil Infrastructure, and Transportation XIII*, 109710E. <https://doi.org/10.1117/12.2514387>.

Nishikawa, T., Yoshida, J., Sugiyama, T. and Fujino, Y., 2012. Concrete crack detection by multiple sequential image filtering. *Computer-Aided Civil and Infrastructure Engineering*, 27(1), pp.29–47.

Piegl, L. and Tiller, W., 1997. Curve and surface fitting. In: *The NURBS Book*. 2nd ed. Berlin: Springer, pp.393–427. Available at: [https://link.springer.com/content/pdf/10.1007/978-3-642-59223-2\\_9.pdf](https://link.springer.com/content/pdf/10.1007/978-3-642-59223-2_9.pdf) [Accessed 10 May 2025].

Rodrigo, R., Eva, D. and Petr, D., 2022. Syncrack: Improving pavement and concrete crack detection through synthetic data generation. In: *17th International Joint Conference on Computer Vision, Imaging and Computer Graphics Theory and Applications (VISAPP'22)*, online, France. Available at: <https://hal.archives-ouvertes.fr/hal-03451685> [Accessed 10 May 2025].

Silverman, R.A., 2002. *Modern Calculus and*

- Analytic Geometry*. Mineola, NY: Dover Publications.
- Shao, Y., Li, L., Li, J., Li, Q., An, S. and Hao, H., 2024. 3DGEN: A framework for generating custom-made synthetic 3D datasets for civil structure health monitoring. *Structural Health Monitoring*. <https://doi.org/10.1177/14759217241265540>
- The Vertikal Press, 2015. Fatal accident during bridge inspection. *Vertikal.net*. Available at: <https://vertikal.net/en/news/story/23700/fatal-accident-during-bridge-inspection> [Accessed 10 May 2025].
- Everett, T.D., Weykamp, P., Capers, H.A., Cox, W.R., Drda, T.S., Hummel, L., Jensen, P., Juntunen, D.A., Kimball, T. and Washer, G.A., 2008. *Bridge Evaluation Quality Assurance in Europe*. Washington, DC: Federal Highway Administration. Available at: <https://international.fhwa.dot.gov/pubs/pl08019/pl08019.pdf> [Accessed 10 May 2025].
- Wu, W., Qi, Z. and Liu, F., 2019. PointConv: Deep convolutional networks on 3D point clouds. In: *Proceedings of the IEEE/CVF Conference on Computer Vision and Pattern Recognition (CVPR)*. Available at: <https://arxiv.org/abs/1811.07246> [Accessed 10 May 2025].
- Wang, M. and Cheng, J.C.P., 2019. A unified convolutional neural network integrated with conditional random field for pipe defect segmentation. *Computer-Aided Civil and Infrastructure Engineering*, 35(2), pp.123–138. <https://doi.org/10.1111/mice.12481>.
- Wei, D., Wang, J. and Zhao, B., 2018. A simple method for particle shape generation with spherical harmonics. *Powder Technology*, 330, pp.284–291. <https://doi.org/10.1016/j.powtec.2018.02.006>
- Valença, J., Puente, I., Júlio, E., González-Jorge, H. and Arias-Sánchez, P., 2017. Assessment of cracks on concrete bridges using image processing supported by laser scanning survey. *Construction and Building Materials*, 146, pp.668–678. <https://doi.org/10.1016/j.conbuildmat.2017.04.096>.